Dipole-dipole-interaction–driven antiblockade of two Rydberg atoms

Shi-Lei Su [1] and Weibin Li [2,*]

[1] *School of Physics, Zhengzhou University, Zhengzhou 450001, China*

[2] *School of Physics and Astronomy, University of Nottingham, Nottingham NG7 2RD, United Kingdom*

(Received 2 August 2021; accepted 13 September 2021; published 27 September 2021)

Resonant laser excitation of multiple Rydberg atoms are prohibited, leading to Rydberg blockade, when the long-range van der Waals interactions are stronger than the laser-atom coupling. Rydberg blockade can be violated, i.e., simultaneous excitation of more than one Rydberg atom, by off-resonant laser excitation, causing an excitation antiblockade. Rydberg antiblockade gives rise to strongly correlated many-body dynamics and spin-orbit coupling and also finds quantum computation applications. Instead of commonly used van der Waals interactions, we investigate antiblockade dynamics of two Rydberg atoms interacting via dipole-dipole exchange interactions. We study typical situations in current Rydberg atom experiments, where different types of dipole-dipole interactions can be achieved by varying Rydberg state couplings. An effective Hamiltonian governing underlying antiblockade dynamics is derived. We illustrate that geometric gates can be realized with the Rydberg antiblockade which is robust against the decay of Rydberg states. Our study may stimulate new experimental and theoretical exploration of quantum optics and strongly interacting many-body dynamics with Rydberg antiblockade driven by dipole-dipole interactions.

DOI: 10.1103/PhysRevA.104.033716

I. INTRODUCTION

Highly excited Rydberg atoms with principal quantum number $n \gg 1$ exhibit strong and long-range van der Waals (vdW) interactions due to their large polarizability ($\sim n^7$) and strong interactions ($\sim n^{11}$) [1]. When excited from ground states with resonant laser lights, a Rydberg blockade emerges in which excitation of two neighboring Rydberg atoms are prohibited due to energy shifts induced by vdW interactions. The Rydberg blockade provides a mechanism for realizing quantum logic gates [2–7], which have been demonstrated experimentally [8–17]. In contrast to a Rydberg blockade, the interaction-induced excitation of two Rydberg atoms is referred to as a *Rydberg antiblockade* (RAB) [18]. Subsequently, the relevant experiment has also observed signatures of Rydberg antiblockades [19]. The strict condition for a RAB was analyzed [20,21]. The RAB plays roles in the study of motional effects [22,23], dissipative dynamics [24–26], periodically driving [27], and quantum computation [28,29]. The RAB was also studied in the detection of structural phase transitions [30], Rydberg spin system [31], cold atom ensembles [32], as well as in strongly interacting Rydberg atom experiments [33].

The vdW and dipole-dipole (DD) interactions exhibit different features. In Fig. 1(a), we show the strength and interaction range of DD and vdW interactions, respectively, focusing on one group of specific Rydberg states. The DD interaction is stronger at short distances, while the vdW interaction is stronger at long distances [7]. Most importantly, DD interactions typically involve two or more Rydberg states in the dynamics. In Fig. 1(b), we show regimes to realize Rydberg blockades [2–4], conventional RABs with simultaneous driving [20,21,23–28,30–32], as well as sequential-driving-based RABs [29], where the excitation conditions can be controlled by laser detuning. When using DD interactions, the density-density as well as spin flip-flop interactions coexist [34,35], leading to complicated many-body dynamics [36]. The resonant DD interactions are considered to construct two- [37] and three-qubit [38] quantum logic gates by using experimentally observed Förster resonances [39]. It has been shown that RABs can be used to limit the blockade error [40] and to construct the multiple-qubit Toffoli and fan-out gates in a fast way [41]. Recently, it has been shown that nonadiabatic dynamics around a conical intersection can be studied under the RAB condition with trapped Rydberg ions [42].

Although there are different level schemes to achieve DD interactions, it is not clear how to achieve the RAB condition for the many types of DD interactions between Rydberg atoms. Moreover, existing schemes typically require two or more Rydberg atoms in the Rydberg state simultaneously for a period of time [37–39,41] or to stay in a dark state [43]. This could reduce the coherence of the system due to, e.g., motional effects [22,23].

In this work we study RAB driven by different types of Rydberg DD interactions. We propose new schemes to realize RAB efficiently for three types of DD interactions that are typically encountered in various experiments. The first type is the Förster resonance, such as transitions given by $|d\rangle|d\rangle \leftrightarrow |p\rangle|f\rangle + |f\rangle|p\rangle$ [44–47], and $|p\rangle|p\rangle \leftrightarrow |s\rangle|s'\rangle + |s'\rangle|s\rangle$ [48,49]. The second type is spin-exchange-type Rydberg-Rydberg interactions (RRIs) via $|s\rangle|p\rangle \leftrightarrow |p\rangle|s\rangle$ [50,51], $|p\rangle|d\rangle \leftrightarrow |d\rangle|p\rangle$ [52], or $|s\rangle|p'\rangle \leftrightarrow |p\rangle|s'\rangle$ [53]. The third type is collective exchange interaction, i.e., $|s\rangle|s'\rangle \leftrightarrow$

*weibin.Li@nottingham.ac.uk

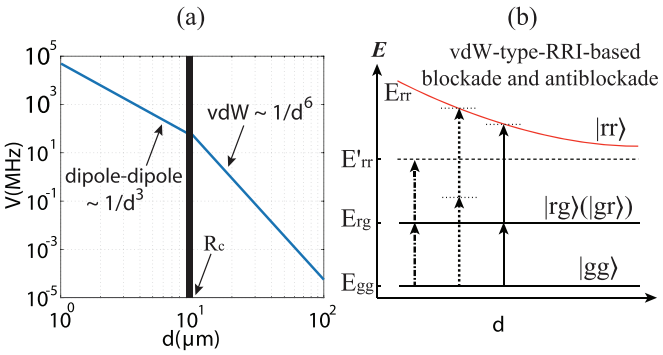

FIG. 1. (a) Two-body interaction strength for Rb atoms excited to Rydberg state $|100s\rangle$ versus interatomic distance d. R_c denotes the crossover distance between DD and vdW interactions [4]. (b) The dynamics of Rydberg blockade and antiblockade with vdW-type RRI. E_{gg}, E_{rg}, and E_{rr} denote the energies of the two-atom state $|gg\rangle$, $|gr\rangle$ ($|rg\rangle$), and $|rr\rangle$, respectively. E'_{rr} denotes the energy when both atoms are excited in Rydberg states but excluding two-body interactions. The resonant laser excitation (dotted-dashed line) leads to the Rydberg blockade [2–4]. The middle excitation process (dotted line) is the conventional Rydberg antiblockade with simultaneous driving [20,21,23–28,30–32]. The right one (solid line) is the RAB with sequential driving [29].

$|p\rangle|p'\rangle$ [37,41,49,54–57]. Effective Hamiltonians of the different types of DD interactions are provided. When applying the proposed schemes in realizing quantum logic gates, the main feature is that only a one-step Rabi oscillation between the ground states and the multi-excited Rydberg states is required, without staying in the Rydberg states for a long period of time, avoiding disadvantages found in other schemes. We also discuss impacts of dissipation on the RAB and propose parameters to probe RABs.

The remaining content of the paper is organized as follows: In Sec. II, we show details on how to achieve the RAB regime. The effective Hamiltonian is given, and the respective dynamics influenced by dissipation is studied with a quantum master equation. We show the population evolution of different models. In Sec. III, the main difference between the vdW and DD interactions are shown, which gives distinctive dynamics. In Sec. IV, we show the potential applications of the proposed RAB in building two-qubit quantum gates and creating steady-state entanglement. The conclusion is given in Sec. V.

II. ANTIBLOCKADE WITH DIFFERENT TYPES OF DD INTERACTIONS

A. Rydberg antiblockade with Förster resonance

1. Level scheme and model

To realize a Förster resonance we consider the experimental configuration [45] $|p\rangle \equiv |61P_{1/2}, m_J = 1/2\rangle$, $|d\rangle \equiv |59D_{3/2}, m_J = 3/2\rangle$, and $|f\rangle \equiv |57F_{5/2}, m_J = 5/2\rangle$ of two ^{87}Rb atoms, as shown in Fig. 2. By applying an electric field $\epsilon = 32$ mV/cm, these Rydberg states can be brought to exact resonance. One of the states in computational space is chosen as $|1\rangle \equiv |5S_{1/2}, F = 2, m_F = 2\rangle$ [45] and the other state $|0\rangle$ in the computational subspace is decoupled with the excitation

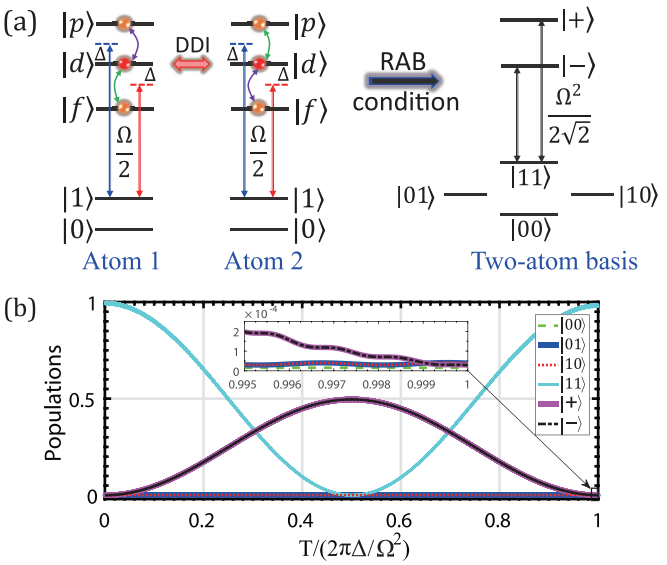

FIG. 2. (a) Left panel shows two Rydberg atoms with resonant RRI. $|0\rangle$ and $|1\rangle$ are two ground states. $|p\rangle$, $|d\rangle$, and $|f\rangle$ are three Rydberg states with the Förster resonance interaction $\hat{H}_d = V_d(|dd\rangle\langle pf| + |dd\rangle\langle fp| + \text{H.c.})$. Right panel gives the effective RAB process in the dressed-state basis. (b) Populations of difference states for RAB scheme in Sec. II A during one evolution period $T = 2\pi\Delta/\Omega^2$ with the consideration of practical atomic spontaneous emission $\gamma_p = 1.89$ kHz, $\gamma_d = 4.55$ kHz, and $\gamma_f = 7.69$ kHz. The inset shows that the dressed state decays to zero at the end of the laser pulse. Parameters are $\Omega = 2\pi \times 5$ MHz and Δ is set to satisfy the antiblockade condition. The initial state is $|11\rangle$ and the interatomic distance is 3 μm.

process and may be chosen as $|0\rangle \equiv |5S_{1/2}, F = 1, m_F = 0\rangle$. The excitation is accomplished by a two-photon process with two lasers with wavelengths 795 nm (π polarization) and 474 nm (σ_+ polarization) [45]. Bichromatic classical fields are imposed on these two atoms to off-resonantly drive the transition $|1\rangle \leftrightarrow |d\rangle$ with an identical Rabi frequency Ω but opposite detuning Δ. With the rotating-wave approximation, the Hamiltonian for this system can be written as $\hat{H} = \hat{H}_\Omega + \hat{H}_d$ ($\hbar \equiv 1$), where

$$\begin{aligned}\hat{H}_\Omega &= \frac{\Omega}{2}(e^{i\Delta t} + e^{-i\Delta t})(|1\rangle_1\langle d| \otimes \mathcal{I}_2 + \mathcal{I}_1 \otimes |1\rangle_2\langle d|) + \text{H.c.}\\ &= \frac{\Omega}{2}(e^{i\Delta t} + e^{-i\Delta t})(|10\rangle\langle d0| + |11\rangle\langle d1| + |1p\rangle\langle dp|\\ &\quad + |1d\rangle\langle dd| + |1f\rangle\langle df| + |01\rangle\langle 0d| + |11\rangle\langle 1d|\\ &\quad + |p1\rangle\langle pd| + |d1\rangle\langle dd| + |f1\rangle\langle fd|) + \text{H.c.},\\ \hat{H}_d &= \sqrt{2}V_d|dd\rangle\langle r_{pf}| + \text{H.c.},\end{aligned} \tag{1}$$

where $\mathcal{I}_j$ denotes the identity matrix of atom j, and $V_d = C_3/r_d^3$ denotes the DD interaction strength. Here $C_3 = 2.54$ GHz μm^3 [45,58] and r_d denotes the interatomic distance. $|mn\rangle$ denotes two atom state $|m\rangle_1 \otimes |n\rangle_2$ and will be used throughout this paper. We have defined two-atom state $|r_{pf}\rangle \equiv (|pf\rangle + |fp\rangle)/\sqrt{2}$.

2. Effective Hamiltonian

To simplify the calculation, we first derive a Hamiltonian using the dressed state basis. It should be mentioned that the dressing here is different from Rydberg dressing of the ground state, which mainly generates long-range interactions between ground-state atoms [59–84]. One can diagonalize $\hat{H}_d$ as $\sqrt{2}V_d(|+\rangle\langle+| - |-\rangle\langle-|)$ with $|\pm\rangle \equiv (|dd\rangle \pm |r_{pf}\rangle)/\sqrt{2}$ being the dressed states. Then the Hamiltonian can be written as

$$\begin{aligned}\hat{H}_\Omega &= \frac{\Omega}{2}(e^{i\Delta t} + e^{-i\Delta t})\big[\sqrt{2}|11\rangle\langle\Psi| + |\Psi\rangle(\langle+| + \langle-|)\big] + \text{H.c.} \\ &\quad + \frac{\Omega}{2}(e^{i\Delta t} + e^{-i\Delta t})(|01\rangle\langle 0d| + |10\rangle\langle d0|) + \text{H.c.}, \\ \hat{H}_d &= \sqrt{2}V_d(|+\rangle\langle+| - |-\rangle\langle-|), \end{aligned} \tag{2}$$

in which $|\Psi\rangle \equiv (|1d\rangle + |d1\rangle)/\sqrt{2}$. From Eq. (2), Hamiltonian $\hat{H}_\Omega$ itself describes resonant interactions when $\Delta = 0$. However, when $V_d \gg \Omega$, after rotating the total Hamiltonian $\hat{H}$ with respect to $\hat{H}_d$, one can see that the two-excitation Rydberg states would be coupled off-resonantly with large detuning. Thus, the Rydberg blockade is produced. In the following we show how to achieve the RAB even when $V_d \gg \Omega$.

When the RRI strength is much stronger than Rabi frequency, the aim is to use the laser detuning to compensate the energy shift induced by the RRI [85]. And it is precisely from this point that one always rotates the whole Hamiltonian with respect to the RRI-related Hamiltonian, which is convenient to get the relation between laser detuning and RRI strength since V_d is also moved to the exponential part (i.e., contributing to the phase) [85,86]. With this at hand, one can employ the second-order perturbation theory to obtain the RAB condition. After rotating the whole Hamiltonian $\hat{H}_\Omega + \hat{H}_d$ with respect to $e^{i\hat{H}_d t}$, this yields [27]

$$\begin{aligned}\hat{\mathcal{H}} = \Big\{ &\frac{\Omega}{2}\big[\sqrt{2}(e^{i\Delta t} + e^{-i\Delta t})|11\rangle\langle\Psi| \\ &+(e^{i(\Delta-\sqrt{2}V_d)t} + e^{-i(\Delta+\sqrt{2}V_d)t})|\Psi\rangle\langle+| \\ &+(e^{i(\Delta+\sqrt{2}V_d)t} + e^{-i(\Delta-\sqrt{2}V_d)t})|\Psi\rangle\langle-| \\ &+(e^{i\Delta t} + e^{-i\Delta t})(|01\rangle\langle 0d| + |10\rangle\langle d0|)\big] + \text{H.c.}\Big\}. \end{aligned} \tag{3}$$

If the conditions $\{\Delta, \Delta \pm \sqrt{2}V_d\} \gg \Omega$, and $V_d = \sqrt{2}\Delta$ are satisfied, the effective form of Hamiltonian (3) can be achieved through the second-order perturbation calculation [87–90] as (see Appendix A for details)

$$\begin{aligned}\hat{H}_e = &\frac{\Omega^2}{2\Delta}|11\rangle\langle+| - |11\rangle\langle-| + \text{H.c.} \\ &+\frac{\Omega^2}{3\Delta}(|+\rangle\langle+| - |-\rangle\langle-|). \end{aligned} \tag{4}$$

From Eq. (4), one can see that the collective ground state $|11\rangle$ is resonantly coupled with the two-excitation Rydberg state $|r_{pf}\rangle$ with effective Rabi frequency $\Omega_{\text{eff}} \equiv \Omega^2/\Delta$, leading to the RAB. Here the Stark shift in Eq. (4) would no doubt influence the dynamics. One can remove the Stark shift by modifying the condition $V_d = \sqrt{2}\Delta$ to

$$V_d = \sqrt{2}\Delta - \Omega^2/\left(3\sqrt{2}\Delta\right),$$

the effective Hamiltonian (4) would be changed to

$$\hat{H}_e = \frac{\Omega^2}{2\sqrt{2}\Delta}|11\rangle(\langle+| - \langle-|) + \text{H.c.} \tag{5}$$

Here we should mention that, in Ref. [45], the ground state $|gg\rangle$ (corresponding to $|11\rangle$ in our paper) is excited to the Rydberg state $|dd\rangle$ first via a π pulse through the detuned laser. Then the electric field is tuned to make state $|dd\rangle$ resonant with $(|pf\rangle + |fp\rangle)/\sqrt{2}$. We consider the strong Förster resonant interactions from the beginning, and designed schemes to achieve the Rabi oscillation from collective ground state to the two-excitation Rydberg state $(|pf\rangle + |fp\rangle)/\sqrt{2}$. Meanwhile, the states $|00\rangle$, $|01\rangle$, and $|10\rangle$ are decoupled with the two-excitation Rydberg states, which is convenient when applying this model for quantum information processing.

3. Population dynamics at the Rydberg antiblockade regime

The effective Hamiltonian (5) shows that perfect Rabi oscillation between the ground state and the doubly excited Rydberg state can happen. In this section, we check the validity of the effective Hamiltonian (5) by comparing dynamics obtained from the original Hamiltonian in the RAB regime. We furthermore take into account spontaneous emission of Rydberg states. The dynamics of the system is governed by the master equation

$$\dot{\hat{\rho}} = i\big[\hat{\rho}, \hat{H}\big] + \frac{1}{2}\sum_k \big[2\hat{\mathcal{L}}_k\hat{\rho}\hat{\mathcal{L}}_k^\dagger - \hat{\mathcal{L}}_k^\dagger\hat{\mathcal{L}}_k\hat{\rho} - \hat{\rho}\hat{\mathcal{L}}_k^\dagger\hat{\mathcal{L}}_k\big], \tag{6}$$

where $\hat{\rho}$ denote the density matrix of system state, $\hat{\mathcal{L}}_k$ is the kth Lindblad operator describing the dissipation process, and $\hat{H} = \hat{H}_\Omega + \hat{V}_d$ is the original Hamiltonian (1). The lifetimes for $|p\rangle$, $|d\rangle$, and $|f\rangle$ are about 0.53, 0.22, and 0.13 ms, respectively [91,92]. The Lindblad operators are given explicitly as

$$\begin{aligned}\hat{\mathcal{L}}_1 &= \sqrt{\gamma_p/2}|0\rangle_1\langle p|, \quad \hat{\mathcal{L}}_2 = \sqrt{\gamma_p/2}|1\rangle_1\langle p|, \\ \hat{\mathcal{L}}_3 &= \sqrt{\gamma_d/2}|0\rangle_1\langle d|, \quad \hat{\mathcal{L}}_4 = \sqrt{\gamma_d/2}|1\rangle_1\langle d|, \\ \hat{\mathcal{L}}_5 &= \sqrt{\gamma_f/2}|0\rangle_1\langle f|, \quad \hat{\mathcal{L}}_6 = \sqrt{\gamma_f/2}|1\rangle_1\langle f|, \\ \hat{\mathcal{L}}_7 &= \sqrt{\gamma_p/2}|0\rangle_2\langle p|, \quad \hat{\mathcal{L}}_8 = \sqrt{\gamma_p/2}|1\rangle_2\langle p|, \\ \hat{\mathcal{L}}_9 &= \sqrt{\gamma_d/2}|0\rangle_2\langle d|, \quad \hat{\mathcal{L}}_{10} = \sqrt{\gamma_d/2}|1\rangle_2\langle d|, \\ \hat{\mathcal{L}}_{11} &= \sqrt{\gamma_f/2}|0\rangle_2\langle f|, \quad \hat{\mathcal{L}}_{12} = \sqrt{\gamma_f/2}|1\rangle_2\langle f|, \end{aligned} \tag{7}$$

where γ_j denotes the atomic spontaneous emission rate.

Numerical results by solving the master equation are shown in Fig. 2(b). The evolution of the state under the given RAB condition is plotted, where the calculation takes into account practical atomic spontaneous emission rates. It can be seen that the initial state can be fully converted to the dressed state, as described by the effective Hamiltonian. Here we should point out that the original Hamiltonian rather than the effective Hamiltonian is used in evolving the master equation. This means that the ideal RAB can be achieved with the DD interaction through the Förster resonance.

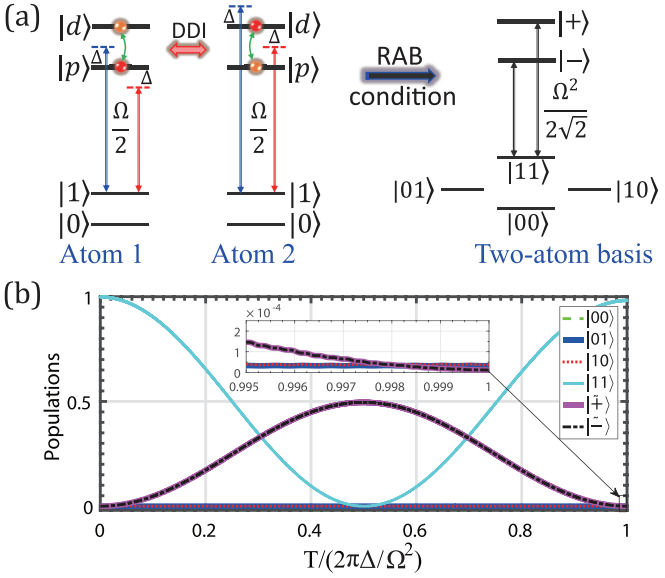

FIG. 3. (a) Left panel shows two Rydberg atoms with DD interactions. $|0\rangle$ and $|1\rangle$ are two ground states. $|p\rangle$ and $|d\rangle$ are two Rydberg states with the spin-exchange interaction $\hat{H}_d = V_d(|pd\rangle\langle dp| + \text{H.c.})$. Right panel shows the effective RAB process in the dressed state basis. (b) Populations of the states for RAB scheme in Sec. II B under one evolution period $T = 2\pi\Delta/\Omega^2$ with the consideration of practical atomic spontaneous emission $\gamma_p = 1.69$ kHz and $\gamma_d = 4$ kHz. Parameters are chosen as $\Omega = 2\pi \times 5$ MHz and Δ is set to satisfy the antiblockade condition. The initial state is set as $|11\rangle$ and the interatomic distance is set as 3 μm.

B. Rydberg antiblockade with spin-exchange interaction

1. Level scheme and model

As shown in Fig. 3, we consider the experimental configuration as [52] $|d\rangle \equiv |62D_{3/2}, m_J = 3/2\rangle$, $|p\rangle \equiv |63P_{1/2}, m_J = 1/2\rangle$. These two Rydberg states are resonant with each other. One of the ground states are chosen as $|1\rangle \equiv |5S_{1/2}, F = 2, m_F = 2\rangle$ [52] and the remaining computational state can be chosen as $|0\rangle \equiv |5S_{1/2}, F = 1, m_F = 0\rangle$. The excitation process from $|1\rangle$ to state $|d\rangle$ is accomplished by a two-photon transition with wavelengths 795 nm (π polarization) and 474 nm (σ_+ polarization), respectively. We also consider the single-photon excitation process from $|1\rangle$ to $|p\rangle$ [52]. For the left (right) Rydberg atom in the left panel, bichromatic classical fields are imposed to off-resonantly drive the transition $|1\rangle \leftrightarrow |p(d)\rangle$ through single-photon (two-photon) process with an identical Rabi frequency Ω but opposite detuning Δ. After the rotating-wave approximation, the Hamiltonian for this concrete system can be written as

$$\begin{aligned}\hat{H}_\Omega &= \frac{\Omega}{2}(e^{i\Delta t} + e^{-i\Delta t})(|1\rangle_1\langle p| \otimes \mathcal{I}_2 + \mathcal{I}_1 \otimes |1\rangle_2\langle d|) + \text{H.c.} \\ &= \frac{\Omega}{2}(e^{i\Delta t} + e^{-i\Delta t})(|10\rangle\langle p0| + |11\rangle\langle p1| + |1p\rangle\langle pp| \\ &\quad + |1d\rangle\langle pd| + |01\rangle\langle 0d| + |11\rangle\langle 1d| + |p1\rangle\langle pd| \\ &\quad + |d1\rangle\langle dd|) + \text{H.c.}, \\ \hat{H}_d &= V_d|pd\rangle\langle dp| + \text{H.c.}, \end{aligned} \tag{8}$$

in which $V_d = C_3/r_d^3$ with C_3 being 7.965 GHz μm^3 here [52,58] and r_d denoting the interatomic distance. In the following we show how to achieve the RAB with this Hamiltonian.

2. Effective Hamiltonian

We first define the dressed states $|\widetilde{\pm}\rangle \equiv (|pd\rangle \pm |dp\rangle)/\sqrt{2}$ by diagonalizing the RRI Hamiltonian. Using the dressed states, one can rewrite Eq. (8) as

$$\begin{aligned}\hat{H}_\Omega &= \frac{\Omega}{\sqrt{2}}(e^{i\Delta t} + e^{-i\Delta t})\left[|11\rangle\langle\Phi| + \frac{1}{\sqrt{2}}|\Phi\rangle(\langle\widetilde{+}| + \langle\widetilde{-}|)\right] \\ &\quad + \frac{\Omega}{2}(e^{i\Delta t} + e^{-i\Delta t})(|01\rangle\langle 0d| + |10\rangle\langle d0|) + \text{H.c.}, \\ \hat{H}_d &= V_d(|\widetilde{+}\rangle\langle\widetilde{+}| - |\widetilde{-}\rangle\langle\widetilde{-}|), \end{aligned} \tag{9}$$

with $|\Phi\rangle \equiv (|1d\rangle + |p1\rangle)/\sqrt{2}$. Following a process similar to that used in Sec. II A and considering $\Delta \gg \Omega$ and RAB condition $V_d = 2\Delta - \Omega^2/(3\Delta)$, we obtain the respective effective Hamiltonian (see Appendix B for details)

$$\hat{H}_e = \frac{\Omega^2}{2\sqrt{2}\Delta}|11\rangle(\langle\widetilde{+}| - \langle\widetilde{-}|) + \text{H.c.}, \tag{10}$$

which means the Rabi oscillation between the collective ground state $|11\rangle$ and the two-excitation Rydberg state $|pf\rangle$ emerges and the RAB can be achieved with an effective π pulse, i.e., $\Omega^2 t/\Delta = \pi$.

Now we discuss the differences in excitation process between our scheme and that in Ref. [52]. In Ref. [52], the atoms are excited step by step. First, one of the Rydberg atoms is excited to the $|d\rangle$ state through a two-photon process. Then the state of the excited Rydberg atom is transferred from $|d\rangle$ to $|p\rangle$ through microwave-field coupling. Immediately, the remaining Rydberg atom is excited to state $|d\rangle$ with $\Omega \simeq 5.76V_d$ and, along with this process, the spin-exchange process also happens. The blockade effect in Ref. [52] does not work because V_d is less than Ω. In our scheme in Sec. II B, by using the dressed state and appropriately choosing the parameters, RAB can be accomplished in one step under the condition $V_d \gg \Omega$.

3. Population dynamics

The full Hamiltonian of the model in Sec. II B is shown in Eq. (8). The lifetimes for $|p\rangle$ and $|d\rangle$ are around 0.59 and 0.25 ms, respectively [91,92]. The resulting master equation is similar. Due to the change of Rydberg levels, the Lindblad operators are changed to

$$\begin{aligned}\hat{\mathcal{L}}_1 &= \sqrt{\gamma_p/2}|0\rangle_1\langle p|, \quad \hat{\mathcal{L}}_2 = \sqrt{\gamma_p/2}|1\rangle_1\langle p|, \\ \hat{\mathcal{L}}_3 &= \sqrt{\gamma_d/2}|0\rangle_1\langle d|, \quad \hat{\mathcal{L}}_4 = \sqrt{\gamma_d/2}|1\rangle_1\langle d|, \\ \hat{\mathcal{L}}_5 &= \sqrt{\gamma_p/2}|0\rangle_2\langle p|, \quad \hat{\mathcal{L}}_6 = \sqrt{\gamma_p/2}|1\rangle_2\langle p|, \\ \hat{\mathcal{L}}_7 &= \sqrt{\gamma_d/2}|0\rangle_2\langle d|, \quad \hat{\mathcal{L}}_8 = \sqrt{\gamma_d/2}|1\rangle_2\langle d|. \end{aligned} \tag{11}$$

In Fig. 3(b), we plot the evolution of the state for the above RAB regime under the given RAB condition by taking into account the decay of Rydberg states. When numerically solving the master equation (6), the original Hamiltonian (8) rather than the effective Hamiltonian is used. As shown in Fig. 3(b),

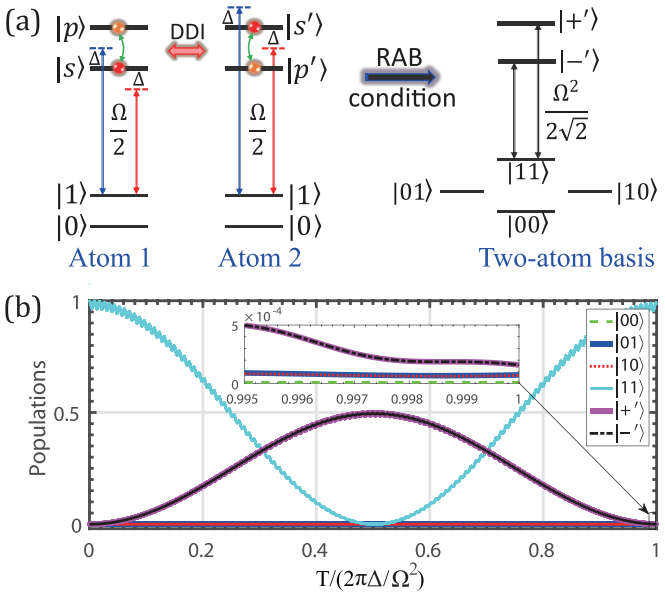

FIG. 4. (a) Left panel shows level scheme of the two Rydberg atoms. $|0\rangle$ and $|1\rangle$ are two ground states. $|s\rangle$ and $|p\rangle$ are two Rydberg states for the left atom, and $|s'\rangle$ and $|p'\rangle$ are two Rydberg states for the right atom. These two Rydberg atoms are interacting each other through the spin-exchange interaction $\hat{H}_d = V_d(|ss'\rangle\langle pp'| + \text{H.c.})$. Right panel shows the effective RAB process in the dressed state basis. (b). Population dynamics for RAB scheme in Sec. II C under one evolution period $T = 2\pi\Delta/\Omega^2$ with atomic spontaneous emission rate $\gamma_s = 8.33$ kHz, $\gamma_{s'} = 7.69$ kHz, $\gamma_p = 4$ kHz, $\gamma_{p'} = 3.7$ kHz. Parameters are $\Omega = 2\pi \times 5$ MHz and Δ is set to satisfy the antiblockade condition. The initial state is $|11\rangle$ and the interatomic distance is 2 μm.

we achieve the RAB such that only the initial and the dressed state participate in the dynamics.

C. Rydberg antiblockade with collective-exchange interaction

1. Level scheme and model

As shown in Fig. 4, we consider two Rydberg atoms, and each has two ground states $|0\rangle$ and $|1\rangle$. The left (right) atom has two Rydberg states $|s\rangle$ and $|p\rangle$ ($|s'\rangle$ and $|p'\rangle$). The experimental configuration is considered as [55] $|s\rangle \equiv |48S_{1/2}, m_J = 1/2\rangle$, $|p\rangle \equiv |48P_{1/2}, m_J = 1/2\rangle$, $|s'\rangle \equiv |50S_{1/2}, m_J = 1/2\rangle$, $|p'\rangle \equiv |49P_{1/2}, m_J = 1/2\rangle$. These states are resonant with each other when applying an electric field $\epsilon = 710$ mV/cm and choosing $r_d = 2$ μm with C_3 to be 0.6 GHz μm^3. Two ground states in computational subspace can be chosen as $|1\rangle \equiv |5S_{1/2}, F = 2, m_F = 0\rangle$ and $|0\rangle \equiv |5S_{1/2}, F = 1, m_F = 0\rangle$ [55]. The excitation from $|1\rangle$ to $|s\rangle$ or $|s'\rangle$ can be implemented by a two-photon process [55].

We consider two bichromatic classical fields are imposed to off-resonantly drive the transition $|1\rangle \leftrightarrow |s(s')\rangle$ with an identical Rabi frequency Ω but opposite detuning Δ. With the rotating-wave approximation, the Hamiltonian for this system can be written by $\hat{H} = \hat{H}_\Omega + \hat{H}_d$, where

$$\begin{aligned}\hat{H}_\Omega &= \frac{\Omega}{2}(e^{i\Delta t} + e^{-i\Delta t})(|1\rangle_1\langle s| \otimes \mathcal{I}_2 + \mathcal{I}_1 \otimes |1\rangle_2\langle s'|) + \text{H.c.}\\ &= \frac{\Omega}{2}(e^{i\Delta t} + e^{-i\Delta t})(|10\rangle\langle s0| + |11\rangle\langle s1| + |1s'\rangle\langle ss'|\\ &\quad + |1p'\rangle\langle sp'| + |01\rangle\langle 0s'| + |11\rangle\langle 1s'| + |s1\rangle\langle ss'|\\ &\quad + |p1\rangle\langle ps'|) + \text{H.c.},\\ \hat{H}_d &= V_d|ss'\rangle\langle pp'| + \text{H.c.} \qquad (12)\end{aligned}$$

As in previous sections, $\hat{H}_\Omega$ and $\hat{H}_d$ describe the laser-atom coupling and the dipole-dipole interaction, respectively.

2. Effective Hamiltonian

To derive the effective Hamiltonian, one can diagonalize the Hamiltonian $\hat{H}_d$ to get the dressed states. Using the respective dressed state, Hamiltonian (12) can be reformulated to be

$$\begin{aligned}\hat{H}_\Omega &= \frac{\Omega}{\sqrt{2}}(e^{i\Delta t} + e^{-i\Delta t})\left[|11\rangle\langle\Xi| + \frac{1}{\sqrt{2}}|\Xi\rangle(\langle +'| + \langle -'|)\right]\\ &\quad + \frac{\Omega}{2}(e^{i\Delta t} + e^{-i\Delta t})(|01\rangle\langle 0s'| + |10\rangle\langle s0|) + \text{H.c.},\\ \hat{H}_d &= V_d(|+'\rangle\langle +'| - |-'\rangle\langle -'|), \qquad (13)\end{aligned}$$

with $|\Xi\rangle \equiv (|1s'\rangle + |s1\rangle)/\sqrt{2}$ and $|\pm'\rangle = (|ss'\rangle \pm |pp'\rangle)/\sqrt{2}$. We find that the RAB condition $V_d = 2\Delta - \Omega^2/(3\Delta)$ can be obtained when $\Delta \gg \Omega$. This leads to the effective Hamiltonian (see Appendix B for details)

$$\hat{H}_e = \frac{\Omega^2}{2\sqrt{2}\Delta}|11\rangle(\langle +'| - \langle -'|) + \text{H.c.}, \qquad (14)$$

which indicates the Rabi oscillation between collective ground state $|11\rangle$ and the two-excitation Rydberg state $|pp'\rangle$. The ground state is completely transferred to the dressed state when $\Omega^2 t/\Delta = \pi$ is fulfilled. In addition to the cases discussed here, the RAB with the resonant DD interaction discussed in Refs. [93,94] can also be realized in a similar way.

In Ref. [55], the optically trapped cloud of 2×10^4 ^{87}Rb gate and source atoms are used for studying the enhancement of single-photon nonlinearity. At zero electric field, the interaction between the $|ss'\rangle$ pair which is of vdW type and much less than the DD interaction. Thus the collective ground state can be excited to $|ss'\rangle$ and the single-photon nonlinearity was observed to be enhanced by electrically tuning $|ss'\rangle$ and $|pp'\rangle$ pair states into resonant interactions [55]. In this section, the resonant DD interaction is an initial consideration and on that basis we design the pulse to achieve the RAB in one step with the condition $V_d \ll \Omega$.

3. Population dynamics

For the model considered in Sec. II C, the full Hamiltonian is shown in Eq. (12). When including the lifetimes for $|s\rangle$, $|s'\rangle$, $|p\rangle$, and $|p'\rangle$, which are 0.12, 0.13, 0.25, and 0.27 ms, respectively [91,92], the dynamics of the system can be obtained by solving the master equation with the following modified Lindblad operators:

$$\begin{aligned}\hat{\mathcal{L}}_1 &= \sqrt{\gamma_s/2}|0\rangle_1\langle s|, \quad \hat{\mathcal{L}}_2 = \sqrt{\gamma_s/2}|1\rangle_1\langle s|,\\ \hat{\mathcal{L}}_3 &= \sqrt{\gamma_p/2}|0\rangle_1\langle p|, \quad \hat{\mathcal{L}}_4 = \sqrt{\gamma_p/2}|1\rangle_1\langle p|,\\ \hat{\mathcal{L}}_5 &= \sqrt{\gamma_{s'}/2}|0\rangle_2\langle s'|, \quad \hat{\mathcal{L}}_6 = \sqrt{\gamma_{s'}/2}|1\rangle_2\langle s'|,\\ \hat{\mathcal{L}}_7 &= \sqrt{\gamma_{p'}/2}|0\rangle_2\langle p'|, \quad \hat{\mathcal{L}}_8 = \sqrt{\gamma_{p'}/2}|1\rangle_2\langle p'|. \qquad (15)\end{aligned}$$

In Fig. 4(b), we plot the evolution of the state for the RAB regime realized with the collective exchange interaction. The finite lifetime in the Rydberg state is taken into account in the simulation. The numerical simulation agrees with the prediction by the effective Hamiltonian nicely, indicating that an ideal RAB regime can be achieved with this type of DD interaction.

III. COMPARISON WITH VAN DER WAALS-INTERACTION-BASED RYDBERG ANTIBLOCKADE

A. Characteristic interatomic distance

For a given Rydberg state, the DD interaction dominates at shorter distances compared with the vdW interaction. Roughly, one can separate the two interactions with a characteristic distance $R_c = [4(C_3)^2/\delta^2]^{1/6}$ [95], where C_3 is the dispersion coefficient, and δ is the detuning of the relevant Rydberg pair states participating in the DD interaction [4,95]. The vdW interaction plays dominant roles when the interatomic distance r is larger than R_c. As a result, one should consider alternative theories to analyze the RAB and related dynamics [20,21,23–28,30–32]. The present work focuses on the regime where the interatomic distance r is less than R_c. As an example, we show the characteristic interatomic distance for $|nS_{1/2}, m_J = 1/2\rangle$ versus principle quantum number n in Fig. 5(a). By fitting the numerical data, it is found that the characteristic distance $R_c \propto n^{3.655}$, agreeing with the scaling analysis in Ref. [95]. It should be noted that here we suppose the channel $2|nS_{1/2}\rangle \to |nP_{1/2}\rangle + |(n-1)P_{1/2}\rangle$ is the dominant channel for simplicity and make numerical calculations. In practice, one might have to consider contributions from all transition channels for evaluating the characteristic distance.

B. Dependence on laser parameters

So far we have assumed that the laser parameters (Rabi frequency and detuning) are constant in deriving the Hamiltonian. In many experiments, fluctuations of the laser parameters cannot be neglected. Importantly, the RAB based on DD and vdW interactions exhibits different responses to the parameter fluctuation. We illustrate the dependence of the two types of interactions by constructing a RAB-based controlled-Z gate. To qualify the fidelity of the gate, we consider the initial state as $|\psi(0)\rangle = (|00\rangle + |01\rangle + |10\rangle + |11\rangle)/4$ and the ideal output state is $|\psi(t)\rangle = (|00\rangle + |01\rangle + |10\rangle - |11\rangle)/4$. The fidelity is then defined as $F = \langle\psi(t)|\rho(t)|\psi(t)\rangle$ throughout this paper. The fidelity of the controlled-Z gate versus the fluctuations of Ω (Δ) is shown in Fig. 5(b) [5(c)]. The gate fidelity based on the DD interaction decreases more slowly than the vdW interaction when increasing the amplitudes of the fluctuations. This example shows that DD-interaction-based RAB has stronger robustness on the parameter fluctuations than vdW-based counterparts in construction of quantum logic gates.

When deriving the effective Hamiltonian via the second-order perturbation theory, the laser detuning should be larger than the Rabi frequency. Meanwhile, the RAB condition sets the relation between the RRI and laser detuning ($V \approx \Delta$). For given Rydberg states, the DD interaction is stronger than the vdW interaction [see Fig. 1(a)], where the range of the allowed Rabi frequency is larger when using the DD interaction than the vdW interaction. To illustrate this, we again examine the performance of the controlled-Z gate by using the DD and vdW interaction. As shown in Fig. 6(a), the gate fidelity drops apparently when increasing Ω in case of the vdW interaction. In contrast, the fidelity decreases slowly with increasing Ω [Fig. 6(b)]. In fact, the fidelity in the latter case is greater than 0.9 for a large range of Ω. This indicates that one can achieve robust controlled-Z gate not only with flexible laser parameters, but can achieve high gate speed using the DD interaction.

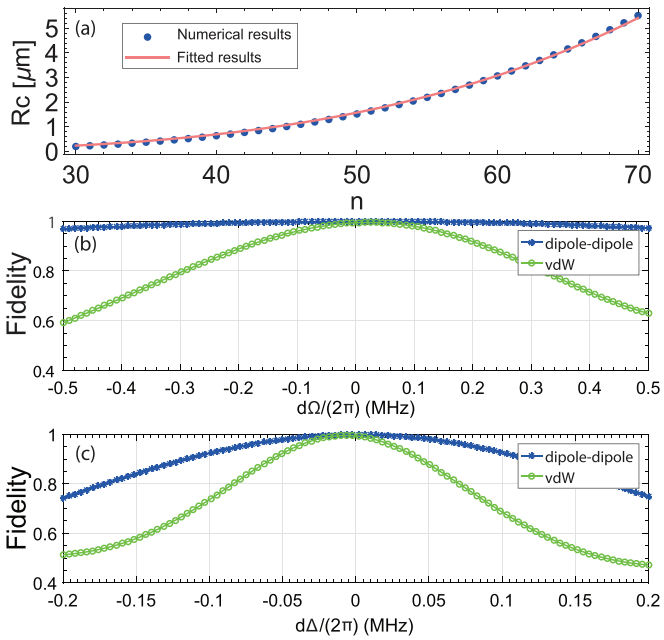

FIG. 5. (a) Characteristic interatomic distance R_c for the state $|nS_{1/2}, m_J = 1/2\rangle$ [95]. Fidelities of the controlled-Z gate versus fluctuations of the laser parameters, i.e., deviations (b) $d\Omega$ and (c) $d\Delta$. For the DD interaction, the energy levels are same as those in Fig. 2 with $\Omega = 2\pi \times 9.9$ MHz, $\gamma_p = 1.89$ kHz, $\gamma_d = 4.55$ kHz, and $\gamma_f = 7.69$ kHz. The interatomic distance is 3 μm, and Δ is determined through the RAB condition given in Sec. II A. For the vdW interaction, the energy levels are the same as those in Fig. 2 without considering $|p\rangle$ and $|f\rangle$ states. The vdW interaction is given by the Hamiltonian $H_{\rm vdW} = C_6/r^6|d\rangle\langle d| \otimes |d\rangle\langle d|$ with $C_6 = 1700$ GHz μm^6 [58] with interatomic distance 6.6 μm. Besides, $\Omega = 2\pi \times 2.2$ MHz, $\gamma_d = 4.55$ kHz, and the RAB condition in Ref. [86] are considered. For panels (b) and (c), the gate time is determined by $T = 2\pi\Delta/\Omega^2$.

C. Dependence on fluctuations of the interatomic distance

In this section, we discuss the influence of the deviation of atom-atom distance on the RAB without setting a concrete energy level. The DD and vdW interactions are given by [4]

$$V_d = \frac{C_3}{r_d^3} \text{ and } V_{\rm vdW} = \frac{C_6}{r_{\rm vdW}^6}, \tag{16}$$

where C_3 and C_6 denote the coefficients of the DD and vdW interactions, respectively. As the vdW and DD interaction have different length scales, we use r_d and $r_{\rm vdW}$ to denote the

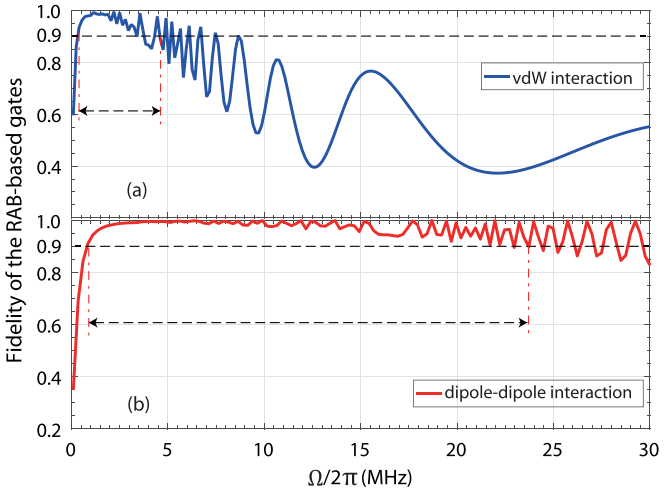

FIG. 6. Fidelities of the controlled-Z gate versus Rabi frequency at the gate time $T = 2\pi\Delta/\Omega^2$. For DD interactions, the energy level and parameters are chosen as that in Fig. 5, except that the Rabi frequency is varied from $2\pi \times 0.5$ to $2\pi \times 30$ MHz. The detuning is chosen to satisfy the RAB condition given in Sec. II A. For vdW interactions, the energy level is the same as that in Fig. 2 without considering $|p\rangle$ and $|f\rangle$ and the RAB condition in given in Ref. [86]. In both cases, the arrow indicates the range of Rabi frequencies where the gate fidelity is larger than 0.9.

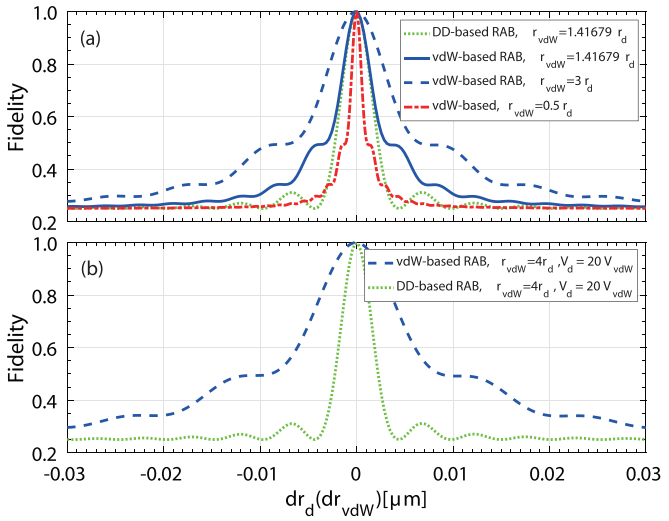

FIG. 7. Fidelity of the RAB-based gates with respect to deviation of interatomic distances at the gate time $T = 2\pi\Delta/\Omega^2$. Panel (a) [(b)] corresponds to case (i) [(ii)] in Sec. III C. Here, $\Omega = 2\pi \times 6.663$ MHz, $\Delta = 10\Omega$, and $r_d = 3$ μm. $V_d = 2\pi \times 94$ MHz. For panel (a) $V_{\rm vdw} = V_d$, while for panel (b), $V_{\rm vdw}$ is shown in the legend of the figure.

interatomic distance. When there is a small deviation in the distance, one can find that the change of the interaction energy are

$$dV_d = -\frac{3V_d}{r_d}dr_d \text{ and } dV_{\rm vdW} = -\frac{6V_{\rm vdW}}{r_{\rm vdW}}dr_{\rm vdW}, \tag{17}$$

where dr_d and $dr_{\rm vdW}$ are small deviations with respect to the interatomic distance. Recently it has been shown that this deviation can lead to interesting many-body phases [30,42,96,97].

To achieve the RAB, the laser detuning has to satisfy the condition $V_d = \sqrt{2}\Delta - \Omega^2/(3\sqrt{2}\Delta)$ in this work and $V_{\rm vdW} = 2\Delta - 2\Omega^2/3\Delta$ in the vdW interaction discussed in Ref. [86]. Thus, a large-interaction-energy shift dV_d and $dV_{\rm vdW}$ will invalidate the RAB condition. To determine the effect of dr_d and $dr_{\rm vdW}$ quantitatively, we consider the following situation: When (i) $V_d = V_{\rm vdW}$ we consider identical deviations of the interatomic distance, i.e., $dr_d = dr_{\rm vdW}$. For the vdW interaction, the detuning Δ has to be adjusted by $0.501\,67dV_{\rm vdW}$ to achieve the RAB. For the DD interaction, Δ need to be adjusted by $0.708\,18dV_d$. Now if we force $0.501\,67dV_{\rm vdW} = 0.708\,18dV_d$, one can derive the relation between the atomic distance, $r_{\rm vdW} \simeq 1.416\,79r_d$. This means that $dV_{\rm vdW}$ is greater than dV_d if $r_{\rm vdW} < 1.416\,79r_d$, and vice versa. When one builds a controlled-Z gate, the DD (vdW) interaction based RAB leads to higher gate fidelity when $r_{\rm vdW} < 1.416\,79r_d$ ($r_{\rm vdW} > 1.416\,79r_d$), as depicted in Fig. 7(a). In the second case (ii) we consider $V_d \gg V_{\rm vdW}$, and $r_d \approx r_{\rm vdW}$. In this case, one can see that $dV_d \gg dV_{\rm vdW}$ is achieved with the same deviation of interatomic distance ($dr_d = dr_{\rm vdW}$). This means the vdW-based RAB is more robust than the DD-interaction case. As depicted in Fig. 7(b), the gate fidelity decreases relatively slowly when using the vdW interaction.

IV. APPLICATIONS OF THE DIPOLE-DIPOLE-INTERACTION–INDUCED RYDBERG ANTIBLOCKADE

Applications of the Rydberg antiblockade have been discussed extensively recently [18–21,23–33,37–41,43,98]. Here we illustrate that the DD-interaction-based RAB can be applied in geometric quantum computation and dissipative dynamics. To be concrete, we focus on the RAB scheme discussed in Sec. II A. It is possible to realize similar applications through other schemes.

A. Two-qubit geometric quantum gate

We first consider how to construct the controlled-arbitrary-phase geometric gate given by the matrix

$$\hat{U}_{\rm CP} = \begin{pmatrix} 1 & 0 & 0 & 0 \\ 0 & 1 & 0 & 0 \\ 0 & 0 & 1 & 0 \\ 0 & 0 & 0 & e^{i\theta} \end{pmatrix} \tag{18}$$

in the computational space $\{|00\rangle, |01\rangle, |10\rangle, |11\rangle\}$. By appropriately modulating the Rabi frequencies of the initial Hamiltonian at the half evolution time $(T/2)$, one can achieve the effective Hamiltonian in the time interval $[T/2, T]$ [87–90],

$$\hat{H}_{\rm e} = -\frac{e^{i\theta}\Omega^2}{2\sqrt{2}\Delta}|11\rangle(\langle +| - \langle -|) + \text{H.c.}, \tag{19}$$

where the phase is controlled by the laser.

The fidelity of the gate is shown in Fig. 8(a) by numerically solving the master equation with the original Hamiltonian, in which the initial state is $|\psi(0)\rangle = (|00\rangle + |01\rangle + |10\rangle + |11\rangle)/4$ and the ideal output state is $|\psi(t)\rangle = \hat{U}|\psi(0)\rangle$. The definition of the fidelity is the same as that in Sec. III B.

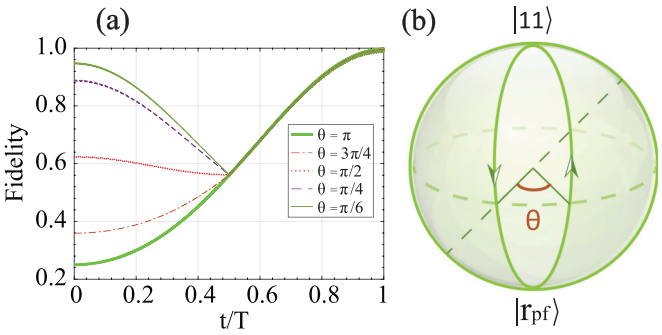

FIG. 8. (a) Evolution of the fidelity of the geometric controlled-arbitrary-phase gate. The parameters are the same as in Fig. 2. (b) Bloch-sphere representation of the geometric quantum operation. The coupling to the dressed state via RAB gives rise to the desired phase shift to the computational basis at the end of the gate operation.

With the consideration of dissipation, the gate fidelity is 0.9969, 0.9962, 0.9949, 0.9938, and 0.9936 when θ equals π, $3\pi/4$, $\pi/2$, $\pi/4$, and $\pi/6$, respectively. The geometric feature of the phase can be easily verified since $|11\rangle \rightarrow |r_{pf}\rangle \rightarrow e^{i\theta}|11\rangle$ is achieved and $\langle\Psi_j|\hat{H}_e|\Psi_k\rangle = 0$ [99–103] is satisfied, where $|\Psi_j\rangle$ ($|\Psi_k\rangle$) is any one of the four states in $\{|00\rangle, |01\rangle, |10\rangle, |11\rangle\}$. Thus, θ is the nonadiabatic geometric phase, which is half of the solid angle enclosed by the evolution path [104], as shown in Fig. 8(b).

B. Steady entanglement

Steady-state entanglement can be created via dissipation in strongly interacting Rydberg systems [24,105]. Following similar ideas, a weak microwave field drives resonantly the transition between two ground states $|0\rangle$ and $|1\rangle$ [Fig. 9(a)],

$$\hat{H}_{\rm mw} = \frac{\sqrt{2}\omega}{2}(|00\rangle + |11\rangle)\langle T| + \text{H.c.}, \tag{20}$$

where $|T\rangle \equiv (|01\rangle + |10\rangle)/\sqrt{2}$ is a triplet Bell state. The singlet state $|S\rangle \equiv (|01\rangle - |10\rangle)/\sqrt{2}$ is decoupled to Hamiltonian (20) and is the desired steady entangled state. We learn from Eq. (20) that the microwave shuffles the states $|00\rangle$, $|T\rangle$, and $|11\rangle$, but keeps $|S\rangle$ invariant. Since the Stark shifts do not influence the dissipative dynamics, we thus consider turning off the red-detuned laser and modifying the RAB condition as $V_d = \sqrt{2}\Delta$. The effective Hamiltonian that control unitary dynamics can be written in the form $\hat{H}'_e = (\Omega'_{\rm eff}/2)(|11\rangle\langle +| + \text{H.c.}) + \hat{S}$, where $\Omega'_{\rm eff} = \sqrt{2}\Omega^2/(2\Delta)$ and $\hat{S}$ denotes the Stark shift.

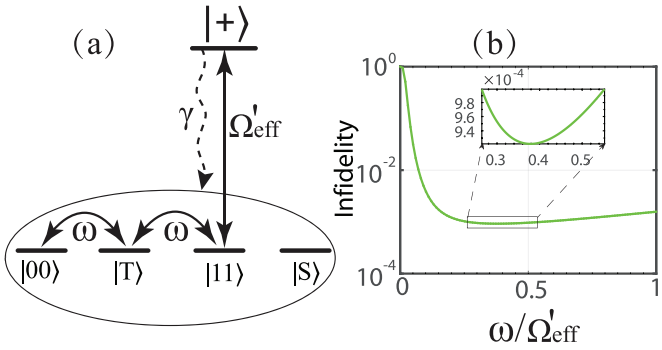

FIG. 9. (a) Dynamical processes to generate the steady entangled state by combining the unitary and dissipative dynamics. (b) Infidelity of the steady entangled state $(|01\rangle - |10\rangle)/\sqrt{2}$ versus $\omega/\Omega'_{\rm eff}$. The interatomic distance is 3 μm, and the Rabi frequency is s $\Omega = 2\pi \times 1$ MHz. Δ is determined through $V_d = \sqrt{2}\Delta$.

Combining the effective Hamiltonian $\hat{H}'_e$ with the microwave Hamiltonian $\hat{H}_{\rm mw}$ in Eq. (20) and the dissipative dynamics as depicted in Fig. 9(a), the desired state $|S\rangle$ would be prepared as the steady state of the system. In other words, once $|S\rangle$ is occupied through the dissipative dynamics, the entangled state is created successfully. Otherwise, if the other three states are occupied, the unitary dynamics will excite the two-atom state to $|r_{pf}\rangle$, which would decay to the ground subspace again. In Fig. 9(b), we plot the infidelity $1 - F$ of the steady state by numerically solving the master equation (6) with the full Hamiltonian, and the practical parameters of RRI and atomic spontaneous emission rate. We find that the fidelity of achieving the desired state can be higher than 0.999.

V. CONCLUSION

In conclusion, we have proposed three schemes to construct the RAB dynamics with different types of DD interactions that are commonly realized in current Rydberg atom experiments. Based on the dressed-state picture, we have derived the effective Hamiltonian that governs the two-atom dynamics. We have verified the validity of the effective Hamiltonian by numerically solving the master equation by taking into account Rydberg state decay. In contrast with the vdW-based RAB due to pure energy shifts by the density-density interaction, our study is valid when the interatomic distance is relatively small, where the DD interaction dominates. In this regime, we have shown that the DD-induced RAB leads to robust dynamics against laser-parameter and interatomic-distance fluctuations.

The DD-induced RAB can be applied to realize various quantum information tasks [18–21,23–33,37–41,43,98] due to the selective two-body excitation process in the underlying dynamics. As examples, we have shown that the proposed RAB can be used in geometric quantum computation and state entanglement preparation. Along with the rapid development in optical trapping [106] and in microwave- [47,53,96,107–109] and electric-field control [3,37,41,44–46,48–50,54–57,93,94,110–112] of the resonant DD RRI, our schemes and the related applications may be tested and realized in future experiments.

ACKNOWLEDGMENTS

S.-L.S. acknowledges support from the Natural Science Foundation of Henan Province (202300410481), National Natural Science Foundation of China (NSFC) under Grant No. 11804308, and the China Postdoctoral Science Foundation (CPSF) under Grant No. 2018T110735. W.L. acknowledges support from the EPSRC through Grant No. EP/R04340X/1 via the QuantERA project "ERyQSenS," the Royal Society Grant No. IEC\NSFC\181078.

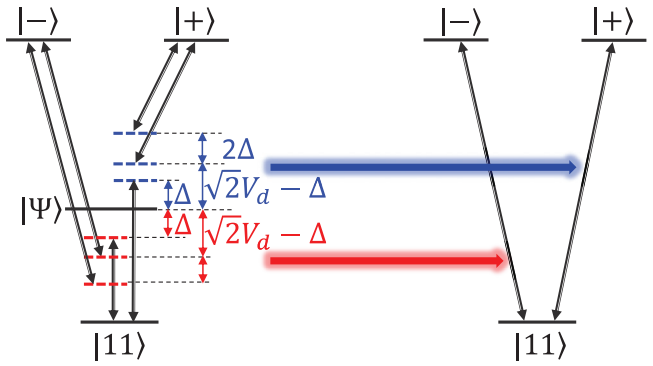

FIG. 10. (left) Dynamical process of Eq. (3) when the initial state is $|11\rangle$. (right) Dynamical process of Eq. (4). The right panel is the effective process of the left panel if the antiblockade condition $\sqrt{2}V_d - \Delta = \Delta$ is satisfied, which is similar to the "two-photon process."

APPENDIX A: DERIVATION OF EQ. (4)

We now show the derivation process of the effective Hamiltonian (4). We start from the rotated Hamiltonian in Eq. (3),

$$\begin{aligned}\hat{\mathcal{H}} = \Big\{ & \frac{\Omega}{2}\big[\sqrt{2}(e^{i\Delta t} + e^{-i\Delta t})|11\rangle\langle\Psi| \\ & + (e^{i(\Delta-\sqrt{2}V_d)t} + e^{-i(\Delta+\sqrt{2}V_d)t})|\Psi\rangle\langle+| \\ & + (e^{i(\Delta+\sqrt{2}V_d)t} + e^{-i(\Delta-\sqrt{2}V_d)t})|\Psi\rangle\langle-| \\ & + (e^{i\Delta t} + e^{-i\Delta t})(|01\rangle\langle 0d| + |10\rangle\langle d0|)\big] + \text{H.c.}\Big\}. \end{aligned} \tag{A1}$$

From Eq. (3), it can be seen that $|11\rangle$ couples with $|\Psi\rangle$ through two channels with detuning Δ and $-\Delta$. Meanwhile, $|\Psi\rangle$ couples with $|\pm\rangle$ through two channels with detuning $\Delta \mp \sqrt{2}V_d$ and $-\Delta \mp \sqrt{2}V_d$, respectively. To be more clearly, in the left panel of Fig. 10, we plot the dynamics of Eq. (3) with the initial state being $|11\rangle$. It can be readily get that if one want to achieve the coupling between $|11\rangle$ and $|+\rangle$ ($|-\rangle$), as shown in the right panel of Fig. 10, via second-order perturbation theory, $\sqrt{2}V_d - \Delta = \Delta$ should be satisfied. On that basis, Eq. (A1) simplifies to

$$\begin{aligned}\hat{\mathcal{H}} = \Big\{ & \frac{\Omega}{2}\big[\sqrt{2}(e^{i\Delta t} + e^{-i\Delta t})|11\rangle\langle\Psi| \\ & + (e^{-i\Delta t} + e^{-i3\Delta t})|\Psi\rangle\langle+| + (e^{i3\Delta t} + e^{i\Delta t})|\Psi\rangle\langle-| \\ & + (e^{i\Delta t} + e^{-i\Delta t})(|01\rangle\langle 0d| + |10\rangle\langle d0|)\big] + \text{H.c.}\Big\}. \end{aligned} \tag{A2}$$

We now show the derivation process of Eq. (4). Based on Fig. 10 and Eqs. (A1) and (A2), one can see that $|+\rangle$ and $|-\rangle$ cannot couple with each other through the intermediate state $|\Psi\rangle$ via second-order perturbation theory. That is because the coupling between $|+\rangle$ and $|-\rangle$ are oscillating with high frequency $e^{i2\Delta t}$ and should be discarded. The Rabi frequency corresponding to the transition between state $|+\rangle$ and state $|11\rangle$ are calculated as

$$\begin{aligned}\frac{\langle+|\hat{\mathcal{H}}|\Psi\rangle\langle\Psi|\hat{\mathcal{H}}|11\rangle}{\Delta} &= \frac{\sqrt{2}\Omega^2}{4\Delta}, \\ \frac{\langle 11|\hat{\mathcal{H}}|\Psi\rangle\langle\Psi|\hat{\mathcal{H}}|+\rangle}{\Delta} &= \frac{\sqrt{2}\Omega^2}{4\Delta}. \end{aligned} \tag{A3}$$

Similarly, the Rabi frequency corresponding to the transition frequency between state $|-\rangle$ and state $|11\rangle$ can be calculated as

$$\begin{aligned}\frac{\langle-|\hat{\mathcal{H}}|\Psi\rangle\langle\Psi|\hat{\mathcal{H}}|11\rangle}{-\Delta} &= \frac{\sqrt{2}\Omega^2}{-4\Delta}, \\ \frac{\langle 11|\hat{\mathcal{H}}|\Psi\rangle\langle\Psi|\hat{\mathcal{H}}|-\rangle}{-\Delta} &= \frac{\sqrt{2}\Omega^2}{-4\Delta}. \end{aligned} \tag{A4}$$

The Stark shifts of state $|+\rangle$, $|-\rangle$, $|10\rangle$, and $|01\rangle$ are

$$\begin{aligned}\frac{\Omega^2}{3\Delta} &= \frac{\langle+|\big(\frac{\Omega}{2}e^{i\Delta t}|+\rangle\langle\Psi|\big)|\Psi\rangle\langle\Psi|\big(\frac{\Omega}{2}e^{-i\Delta t}|\Psi\rangle\langle+|\big)|+\rangle}{\Delta} + \frac{\langle+|\big(\frac{\Omega}{2}e^{i3\Delta t}|+\rangle\langle\Psi|\big)|\Psi\rangle\langle\Psi|\big(\frac{\Omega}{2}e^{-i3\Delta t}|\Psi\rangle\langle+|\big)|+\rangle}{3\Delta}, \\ \frac{\Omega^2}{-3\Delta} &= \frac{\langle-|\big(\frac{\Omega}{2}e^{-i\Delta t}|-\rangle\langle\Psi|\big)|\Psi\rangle\langle\Psi|\big(\frac{\Omega}{2}e^{i\Delta t}|\Psi\rangle\langle+|\big)|+\rangle}{-\Delta} + \frac{\langle+|\big(\frac{\Omega}{2}e^{-i3\Delta t}|-\rangle\langle\Psi|\big)|\Psi\rangle\langle\Psi|\big(\frac{\Omega}{2}e^{i3\Delta t}|\Psi\rangle\langle-|\big)|-\rangle}{-3\Delta}, \\ 0 &= \frac{\langle 10|\big(\frac{\Omega}{2}e^{i\Delta t}|10\rangle\langle d0|\big)|d0\rangle\langle d0|\big(\frac{\Omega}{2}e^{-i\Delta t}|d0\rangle\langle 10|\big)|10\rangle}{\Delta} + \frac{\langle 10|\big(\frac{\Omega}{2}e^{-i\Delta t}|10\rangle\langle d0|\big)|d0\rangle\langle d0|\big(\frac{\Omega}{2}e^{i\Delta t}|d0\rangle\langle 10|\big)|10\rangle}{-\Delta}, \\ 0 &= \frac{\langle 01|\big(\frac{\Omega}{2}e^{i\Delta t}|01\rangle\langle 0d|\big)|0d\rangle\langle 0d|\big(\frac{\Omega}{2}e^{-i\Delta t}|0d\rangle\langle 01|\big)|01\rangle}{\Delta} + \frac{\langle 01|\big(\frac{\Omega}{2}e^{-i\Delta t}|01\rangle\langle 0d|\big)|0d\rangle\langle 0d|\big(\frac{\Omega}{2}e^{i\Delta t}|0d\rangle\langle 01|\big)|01\rangle}{-\Delta}, \end{aligned} \tag{A5}$$

respectively. Besides, the coupling between $|10\rangle$ ($|01\rangle$) and the single-excited state is large detuned and should be discarded. Besides, it should be noted that it is needless to calculate the Stark shift of $|\Psi\rangle$ since it is also discarded due to the large detuning condition. So the effective Hamiltonian of the system can be written as

$$\hat{H}_e = \frac{\sqrt{2}\Omega^2}{4\Delta}(|11\rangle\langle+| - |11\rangle\langle-| + \text{H.c.}) + \frac{\Omega^2}{3\Delta}(|+\rangle\langle+| - |-\rangle\langle-|), \tag{A6}$$

which is exactly Eq. (4).

APPENDIX B: DERIVATION OF EQ. (10)

Following a similar process, Eqs. (10) and (14) can also be achieved with the corresponding given antiblockade conditions. Alternatively, here we use another method [87–90] based on time averaging to calculate the effective Hamiltonian (10). First, we rotate the whole Hamiltonian with respect to

$\hat{U} = e^{i2\Delta(|\widetilde{+}\rangle\langle\widetilde{+}|-|\widetilde{-}\rangle\langle\widetilde{-}|)t}$. The total Hamiltonian in the rotated frame is then changed to

$$\begin{aligned}\hat{H}_{\text{rotate}} = &\frac{\Omega}{\sqrt{2}}(e^{i\Delta t}+e^{-i\Delta t})|11\rangle\langle\Phi| + \frac{\Omega}{2}(e^{-i\Delta t}+e^{-i3\Delta t})|\Phi\rangle\langle\widetilde{+}| + \frac{\Omega}{2}(e^{i3\Delta t}+e^{i\Delta t})|\Phi\rangle\langle\widetilde{-}| \\ &+ \frac{\Omega}{2}(e^{i\Delta t}+e^{-i\Delta t})(|01\rangle\langle 0d| + |10\rangle\langle d0|) + \text{H.c.} + (V_d - 2\Delta)(|\widetilde{+}\rangle\langle\widetilde{+}| - |\widetilde{-}\rangle\langle\widetilde{-}|). \end{aligned} \tag{B1}$$

We now briefly review the effective Hamiltonian formula in Refs. [87–90]. For a Hamiltonian in the interaction picture,

$$\hat{H} = \sum_{n=1}^{N} \hat{h}_n^{\dagger} e^{i\omega_n t} + \hat{h}_n e^{-i\omega_n t}, \tag{B2}$$

if the large-detuning condition is satisfied, the effective Hamiltonian would be

$$\hat{H}_{\text{eff}} = \sum_{m,n=1}^{N} \frac{1}{\hbar\overline{\omega_{mn}}}\left[\hat{h}_m^{\dagger}, \hat{h}_n\right] e^{i(\omega_m-\omega_n)t}, \tag{B3}$$

where $\overline{\omega_{mn}} = 2\omega_m\omega_n/(\omega_m+\omega_n)$. After using Eq. (B2), the processes to calculate the effective form of Eq. (B1) are as follows:

$$\begin{aligned}
\frac{\Omega^2}{2\sqrt{2}\Delta}\left[|11\rangle\langle\Phi|e^{i\Delta t}, |\Phi\rangle\langle\widetilde{+}|e^{-i\Delta t}\right]e^{i(\Delta-\Delta)t} &= \frac{\Omega^2}{2\sqrt{2}\Delta}|11\rangle\langle\widetilde{+}|, \\
\frac{\Omega^2}{2\sqrt{2}\Delta}\left[|\Phi\rangle\langle 11|e^{i\Delta t}, |\widetilde{-}\rangle\langle\Phi|e^{-i\Delta t}\right]e^{i(\Delta-\Delta)t} &= -\frac{\Omega^2}{2\sqrt{2}\Delta}|\widetilde{-}\rangle\langle 11|, \\
\frac{\Omega^2}{2\sqrt{2}\Delta}\left[|\widetilde{+}\rangle\langle\Phi|e^{i\Delta t}, |\Phi\rangle\langle 11|e^{-i\Delta t}\right]e^{i(\Delta-\Delta)t} &= \frac{\Omega^2}{2\sqrt{2}\Delta}|\widetilde{+}\rangle\langle 11|, \\
\frac{\Omega^2}{2\sqrt{2}\Delta}\left[|\Phi\rangle\langle\widetilde{-}|e^{i\Delta t}, |11\rangle\langle\Phi|e^{-i\Delta t}\right]e^{i(\Delta-\Delta)t} &= -\frac{\Omega^2}{2\sqrt{2}\Delta}|11\rangle\langle\widetilde{-}|, \\
\frac{\Omega^2}{2\Delta}\left[|11\rangle\langle\Phi|e^{i\Delta t}, |\Phi\rangle\langle 11|e^{-i\Delta t}\right]e^{i(\Delta-\Delta)t} &= \frac{\Omega^2}{2\Delta}(|11\rangle\langle 11| - |\Phi\rangle\langle\Phi|), \\
\frac{\Omega^2}{2\Delta}\left[|\Phi\rangle\langle 11|e^{i\Delta t}, |11\rangle\langle\Phi|e^{-i\Delta t}\right]e^{i(\Delta-\Delta)t} &= \frac{\Omega^2}{2\Delta}(|\Phi\rangle\langle\Phi| - |11\rangle\langle 11|), \\
\frac{\Omega^2}{4\Delta}\left[|\widetilde{+}\rangle\langle\Phi|e^{i\Delta t}, |\Phi\rangle|\widetilde{+}|e^{-i\Delta t}\right]e^{i(\Delta-\Delta)t} &= \frac{\Omega^2}{4\Delta}(|\widetilde{+}\rangle\langle\widetilde{+}| - |\Phi\rangle\langle\Phi|), \\
\frac{\Omega^2}{12\Delta}\left[|\widetilde{+}\rangle\langle\Phi|e^{i3\Delta t}, |\Phi\rangle|\widetilde{+}\rangle|e^{-i3\Delta t}\right]e^{i(3\Delta-3\Delta)t} &= \frac{\Omega^2}{12\Delta}(|\widetilde{+}\rangle\langle\widetilde{+}| - |\Phi\rangle\langle\Phi|), \\
\frac{\Omega^2}{12\Delta}\left[|\Phi\rangle\langle\widetilde{-}|e^{i3\Delta t}, |\widetilde{-}\rangle\langle\Phi|e^{-i3\Delta t}\right]e^{i(3\Delta-3\Delta)t} &= \frac{\Omega^2}{12\Delta}(|\Phi\rangle\langle\Phi| - |\widetilde{-}\rangle\langle\widetilde{-}|), \\
\frac{\Omega^2}{4\Delta}\left[|\Phi\rangle\langle\widetilde{-}|e^{i\Delta t}, |\widetilde{-}\rangle\langle\Phi|e^{-i\Delta t}\right]e^{i(\Delta-\Delta)t} &= \frac{\Omega^2}{4\Delta}(|\Phi\rangle\langle\Phi| - |\widetilde{-}\rangle\langle\widetilde{-}|), \\
\frac{\Omega^2}{4\Delta}\left[(|01\rangle\langle 0d| + |10\rangle\langle d0|)e^{i\Delta t}, (|0d\rangle\langle 01| + |d0\rangle\langle 10|)e^{-i\Delta t}\right]e^{i(\Delta-\Delta)t} &= \frac{\Omega^2}{4\Delta}(|01\rangle\langle 01| - |0d\rangle\langle 0d|), \\
\frac{\Omega^2}{4\Delta}\left[(|0d\rangle\langle 01| + |d0\rangle\langle 10|)e^{i\Delta t}, (|01\rangle\langle 0d| + |10\rangle\langle d0|)e^{-i\Delta t}\right]e^{i(\Delta-\Delta)t} &= \frac{\Omega^2}{4\Delta}(|0d\rangle\langle 0d| - |01\rangle\langle 01|).
\end{aligned} \tag{B4}$$

It should be noted that the high-frequency oscillation terms are discarded and were not shown in Eq. (B4). The sum of the terms in Eq. (B4) induces the effective Hamiltonian as

$$\begin{aligned}\hat{H}_e = &\frac{\Omega^2}{2\sqrt{2}\Delta}(|11\rangle\langle\widetilde{+}| - |11\rangle\langle\widetilde{-}| + \text{H.c.}) \\ &+ \frac{\Omega^2}{3\Delta}(|\widetilde{+}\rangle\langle\widetilde{+}| - |\widetilde{-}\rangle\langle\widetilde{-}|) \\ &+ (V_d - 2\Delta)(|\widetilde{+}\rangle\langle\widetilde{+}| - |\widetilde{-}\rangle\langle\widetilde{-}|), \end{aligned} \tag{B5}$$

in which the Stark shift terms of state $|\widetilde{+}\rangle$ and state $|\widetilde{-}\rangle$ exactly cancel out $(V_d - 2\Delta)(|\widetilde{+}\rangle\langle\widetilde{+}| - |\widetilde{-}\rangle\langle\widetilde{-}|)$ when the antiblockade condition $V_d = 2\Delta - \Omega^2/(3\Delta)$ is satisfied. After using $|\widetilde{\pm}\rangle \equiv (|pd\rangle \pm |dp\rangle)/\sqrt{2}$ the total effective Hamiltonian of the system in the rotated frame becomes

$$\hat{H}_{\text{e}} = \frac{\Omega^2}{2\Delta}|11\rangle\langle dp| + \text{H.c.}, \tag{B6}$$

which means Eq. (10) is achieved. Similarly, to deviate Eq. (14), either one of the above two methods are feasible.

[1] T. F. Gallagher, *Rydberg Atoms* (Cambridge University Press, Cambridge, 2005).

[2] D. Jaksch, J. I. Cirac, P. Zoller, S. L. Rolston, R. Côté, and M. D. Lukin, Phys. Rev. Lett. **85**, 2208 (2000).

[3] M. D. Lukin, M. Fleischhauer, R. Cote, L. M. Duan, D. Jaksch, J. I. Cirac, and P. Zoller, Phys. Rev. Lett. **87**, 037901 (2001).

[4] M. Saffman, T. G. Walker, and K. Mølmer, Rev. Mod. Phys. **82**, 2313 (2010).

[5] D. Comparat and P. Pillet, J. Opt. Soc. Am. B **27**, A208 (2010).

[6] W. Li and I. Lesanovsky, Appl. Phys. B: Lasers Opt. **114**, 37 (2014).

[7] M. Saffman, J. Phys. B: At., Mol. Opt. Phys. **49**, 202001 (2016).

[8] L. Isenhower, E. Urban, X. L. Zhang, A. T. Gill, T. Henage, T. A. Johnson, T. G. Walker, and M. Saffman, Phys. Rev. Lett. **104**, 010503 (2010).

[9] X. L. Zhang, L. Isenhower, A. T. Gill, T. G. Walker, and M. Saffman, Phys. Rev. A **82**, 030306(R) (2010).

[10] T. Wilk, A. Gaëtan, C. Evellin, J. Wolters, Y. Miroshnychenko, P. Grangier, and A. Browaeys, Phys. Rev. Lett. **104**, 010502 (2010).

[11] K. M. Maller, M. T. Lichtman, T. Xia, Y. Sun, M. J. Piotrowicz, A. W. Carr, L. Isenhower, and M. Saffman, Phys. Rev. A **92**, 022336 (2015).

[12] Y. Zeng, P. Xu, X. He, Y. Liu, M. Liu, J. Wang, D. J. Papoular, G. V. Shlyapnikov, and M. Zhan, Phys. Rev. Lett. **119**, 160502 (2017).

[13] C. J. Picken, R. Legaie, K. McDonnell, and J. D. Pritchard, Quantum Sci. Technol. **4**, 015011 (2018).

[14] H. Levine, A. Keesling, A. Omran, H. Bernien, S. Schwartz, A. S. Zibrov, M. Endres, M. Greiner, V. Vuletić, and M. D. Lukin, Phys. Rev. Lett. **121**, 123603 (2018).

[15] H. Levine, A. Keesling, G. Semeghini, A. Omran, T. T. Wang, S. Ebadi, H. Bernien, M. Greiner, V. Vuletić, H. Pichler, and M. D. Lukin, Phys. Rev. Lett. **123**, 170503 (2019).

[16] T. M. Graham, M. Kwon, B. Grinkemeyer, Z. Marra, X. Jiang, M. T. Lichtman, Y. Sun, M. Ebert, and M. Saffman, Phys. Rev. Lett. **123**, 230501 (2019).

[17] A. Omran, H. Levine, A. Keesling, G. Semeghini, T. T. Wang, S. Ebadi, H. Bernien, A. S. Zibrov, H. Pichler, S. Choi, J. Cui, M. Rossignolo, P. Rembold, S. Montangero, T. Calarco, M. Endres, M. Greiner, V. Vuletić, and M. D. Lukin, Science **365**, 570 (2019).

[18] C. Ates, T. Pohl, T. Pattard, and J. M. Rost, Phys. Rev. Lett. **98**, 023002 (2007).

[19] T. Amthor, C. Giese, C. S. Hofmann, and M. Weidemüller, Phys. Rev. Lett. **104**, 013001 (2010).

[20] Z. Zuo and K. Nakagawa, Phys. Rev. A **82**, 062328 (2010).

[21] T. E. Lee, H. Häffner, and M. C. Cross, Phys. Rev. Lett. **108**, 023602 (2012).

[22] C. Ates, B. Olmos, W. Li, and I. Lesanovsky, Phys. Rev. Lett. **109**, 233003 (2012).

[23] W. Li, C. Ates, and I. Lesanovsky, Phys. Rev. Lett. **110**, 213005 (2013).

[24] A. W. Carr and M. Saffman, Phys. Rev. Lett. **111**, 033607 (2013).

[25] Y.-H. Chen, Z.-C. Shi, J. Song, Y. Xia, and S.-B. Zheng, Phys. Rev. A **97**, 032328 (2018); D. X. Li and X. Q. Shao, *ibid.* **99**, 032348 (2019); C. Yang, D. Li, and X. Shao, Sci. China: Phys., Mech. Astron. **62**, 110312 (2019).

[26] R. Li, D. Yu, S.-L. Su, and J. Qian, Phys. Rev. A **101**, 042328 (2020).

[27] S. Basak, Y. Chougale, and R. Nath, Phys. Rev. Lett. **120**, 123204 (2018).

[28] S. L. Su, H. Z. Shen, E. Liang, and S. Zhang, Phys. Rev. A **98**, 032306 (2018); S.-L. Su, F.-Q. Guo, L. Tian, X.-Y. Zhu, L.-L. Yan, E.-J. Liang, and M. Feng, *ibid.* **101**, 012347 (2020); J.-L. Wu, S.-L. Su, Y. Wang, J. Song, Y. Xia, and Y.-Y. Jiang, Opt. Lett. **45**, 1200 (2020); R.-H. Zheng, Y.-H. Kang, S.-L. Su, J. Song, and Y. Xia, Phys. Rev. A **102**, 012609 (2020).

[29] S.-L. Su, Y. Gao, E. Liang, and S. Zhang, Phys. Rev. A **95**, 022319 (2017).

[30] F. M. Gambetta, C. Zhang, M. Hennrich, I. Lesanovsky, and W. Li, Phys. Rev. Lett. **125**, 133602 (2020).

[31] P. P. Mazza, R. Schmidt, and I. Lesanovsky, Phys. Rev. Lett. **125**, 033602 (2020).

[32] J. Taylor, J. Sinclair, K. Bonsma-Fisher, D. England, M. Spanner, and K. Heshami, arXiv:1912.05675.

[33] S. Bai, X. Tian, X. Han, Y. Jiao, J. Wu, J. Zhao, and S. Jia, New J. Phys. **22**, 013004 (2020).

[34] A. Cidrim, T. S. do Espirito Santo, J. Schachenmayer, R. Kaiser, and R. Bachelard, Phys. Rev. Lett. **125**, 073601 (2020).

[35] L. A. Williamson, M. O. Borgh, and J. Ruostekoski, Phys. Rev. Lett. **125**, 073602 (2020).

[36] A. P. Orioli, A. Signoles, H. Wildhagen, G. Günter, J. Berges, S. Whitlock, and M. Weidemüller, Phys. Rev. Lett. **120**, 063601 (2018).

[37] I. I. Beterov, M. Saffman, E. A. Yakshina, D. B. Tretyakov, V. M. Entin, S. Bergamini, E. A. Kuznetsova, and I. I. Ryabtsev, Phys. Rev. A **94**, 062307 (2016).

[38] I. I. Beterov, I. N. Ashkarin, E. A. Yakshina, D. B. Tretyakov, V. M. Entin, I. I. Ryabtsev, P. Cheinet, P. Pillet, and M. Saffman, Phys. Rev. A **98**, 042704 (2018).

[39] D. B. Tretyakov, I. I. Beterov, E. A. Yakshina, V. M. Entin, I. I. Ryabtsev, P. Cheinet, and P. Pillet, Phys. Rev. Lett. **119**, 173402 (2017).

[40] X.-F. Shi, Phys. Rev. Appl. **7**, 064017 (2017).

[41] M. Khazali and K. Mølmer, Phys. Rev. X **10**, 021054 (2020).

[42] F. M. Gambetta, C. Zhang, M. Hennrich, I. Lesanovsky, and W. Li, Phys. Rev. Lett. **126**, 233404 (2021).

[43] T. Pohl and P. R. Berman, Phys. Rev. Lett. **102**, 013004 (2009).

[44] J. Nipper, J. B. Balewski, A. T. Krupp, B. Butscher, R. Löw, and T. Pfau, Phys. Rev. Lett. **108**, 113001 (2012).

[45] S. Ravets, H. Labuhn, D. Barredo, L. Béguin, T. Lahaye, and A. Browaeys, Nat. Phys. **10**, 914 (2014).

[46] S. Ravets, H. Labuhn, D. Barredo, T. Lahaye, and A. Browaeys, Phys. Rev. A **92**, 020701(R) (2015).

[47] P. Bohlouli-Zanjani, J. A. Petrus, and J. D. D. Martin, Phys. Rev. Lett. **98**, 203005 (2007).

[48] E. A. Yakshina, D. B. Tretyakov, I. I. Beterov, V. M. Entin, C. Andreeva, A. Cinins, A. Markovski, Z. Iftikhar, A. Ekers, and I. I. Ryabtsev, Phys. Rev. A **94**, 043417 (2016).

[49] Z. C. Liu, N. P. Inman, T. J. Carroll, and M. W. Noel, Phys. Rev. Lett. **124**, 133402 (2020).

[50] A. Browaeys, D. Barredo, and T. Lahaye, J. Phys. B: At., Mol. Opt. Phys. **49**, 152001 (2016).

[51] C. Ates, A. Eisfeld, and J. M. Rost, New J. Phys. **10**, 045030 (2008).

[52] D. Barredo, H. Labuhn, S. Ravets, T. Lahaye, A. Browaeys, and C. S. Adams, Phys. Rev. Lett. **114**, 113002 (2015).

[53] J. T. Young, P. Bienias, R. Belyansky, A. M. Kaufman, and A. V. Gorshkov, Asymmetric blockade and multi-qubit gates via dipole-dipole interactions, Phys. Rev. Lett. **127**, 120501 (2021).

[54] W. R. Anderson, J. R. Veale, and T. F. Gallagher, Phys. Rev. Lett. **80**, 249 (1998).

[55] H. Gorniaczyk, C. Tresp, P. Bienias, A. Paris-Mandoki, W. Li, I. Mirgorodskiy, H. P. Büchler, I. Lesanovsky, and S. Hofferberth, Nat. Commun. **7**, 12480 (2016).

[56] D. Petrosyan, F. Motzoi, M. Saffman, and K. Mølmer, Phys. Rev. A **96**, 042306 (2017).

[57] I. I. Beterov, G. N. Khamzina, D. B. Tret'yakov, V. M. Entin, E. A. Yakshina, and I. I. Ryabtsev, Quantum Electron. **48**, 453 (2018).

[58] K. Singer, J. Stanojevic, M. Weidemüller, and R. Côté, J. Phys. B: At., Mol. Opt. Phys. **38**, S295 (2005); B. Olmos, W. Li, S. Hofferberth, and I. Lesanovsky, Phys. Rev. A **84**, 041607(R) (2011); N. Šibalić, J. Pritchard, C. Adams, and K. Weatherill, Comput. Phys. Commun. **220**, 319 (2017).

[59] G. Pupillo, A. Micheli, M. Boninsegni, I. Lesanovsky, and P. Zoller, Phys. Rev. Lett. **104**, 223002 (2010).

[60] Y.-Y. Jau, A. M. Hankin, T. Keating, I. H. Deutsch, and G. W. Biedermann, Nat. Phys. **12**, 71 (2016).

[61] J. Zeiher, R. van Bijnen, P. Schauß, S. Hild, J.-y. Choi, T. Pohl, I. Bloch, and C. Gross, Nat. Phys. **12**, 1095 (2016).

[62] J. Honer, H. Weimer, T. Pfau, and H. P. Büchler, Phys. Rev. Lett. **105**, 160404 (2010).

[63] A. W. Glaetzle, M. Dalmonte, R. Nath, C. Gross, I. Bloch, and P. Zoller, Phys. Rev. Lett. **114**, 173002 (2015).

[64] J. E. Johnson and S. L. Rolston, Phys. Rev. A **82**, 033412 (2010).

[65] R. M. W. van Bijnen and T. Pohl, Phys. Rev. Lett. **114**, 243002 (2015).

[66] J. B. Balewski, A. T. Krupp, A. Gaj, S. Hofferberth, R. Löw, and T. Pfau, New J. Phys. **16**, 063012 (2014).

[67] N. Henkel, F. Cinti, P. Jain, G. Pupillo, and T. Pohl, Phys. Rev. Lett. **108**, 265301 (2012).

[68] H. Schempp, G. Günter, S. Wüster, M. Weidemüller, and S. Whitlock, Phys. Rev. Lett. **115**, 093002 (2015).

[69] M. Tanasittikosol, J. D. Pritchard, D. Maxwell, A. Gauguet, K. J. Weatherill, R. M. Potvliege, and C. S. Adams, J. Phys. B: At., Mol. Opt. Phys. **44**, 184020 (2011).

[70] T. Macrì and T. Pohl, Phys. Rev. A **89**, 011402(R) (2014).

[71] T. Keating, K. Goyal, Y.-Y. Jau, G. W. Biedermann, A. J. Landahl, and I. H. Deutsch, Phys. Rev. A **87**, 052314 (2013).

[72] S. Wüster, C. Ates, A. Eisfeld, and J. M. Rost, New J. Phys. **13**, 073044 (2011).

[73] T. Keating, R. L. Cook, A. M. Hankin, Y.-Y. Jau, G. W. Biedermann, and I. H. Deutsch, Phys. Rev. A **91**, 012337 (2015).

[74] M. Mattioli, M. Dalmonte, W. Lechner, and G. Pupillo, Phys. Rev. Lett. **111**, 165302 (2013).

[75] W. Li, L. Hamadeh, and I. Lesanovsky, Phys. Rev. A **85**, 053615 (2012).

[76] C. Gaul, B. J. DeSalvo, J. A. Aman, F. B. Dunning, T. C. Killian, and T. Pohl, Phys. Rev. Lett. **116**, 243001 (2016).

[77] D. Petrosyan and K. Mølmer, Phys. Rev. Lett. **113**, 123003 (2014).

[78] R. Mukherjee, C. Ates, W. Li, and S. Wüster, Phys. Rev. Lett. **115**, 040401 (2015).

[79] L. F. Buchmann, K. Mølmer, and D. Petrosyan, Phys. Rev. A **95**, 013403 (2017).

[80] Y. Li, A. Geißler, W. Hofstetter, and W. Li, Phys. Rev. A **97**, 023619 (2018).

[81] J. Lee, M. J. Martin, Y.-Y. Jau, T. Keating, I. H. Deutsch, and G. W. Biedermann, Phys. Rev. A **95**, 041801(R) (2017).

[82] Y. Zhou, Y. Li, R. Nath, and W. Li, Phys. Rev. A **101**, 013427 (2020).

[83] G. McCormack, R. Nath, and W. Li, Phys. Rev. A **102**, 023319 (2020).

[84] Y. Li, H. Cai, D.-w. Wang, L. Li, J. Yuan, and W. Li, Phys. Rev. Lett. **124**, 140401 (2020).

[85] S.-L. Su, F.-Q. Guo, J.-L. Wu, Z. Jin, X. Q. Shao, and S. Zhang, Europhys. Lett. **131**, 53001 (2020).

[86] S.-L. Su, E. Liang, S. Zhang, J.-J. Wen, L.-L. Sun, Z. Jin, and A.-D. Zhu, Phys. Rev. A **93**, 012306 (2016).

[87] D. James, Fortschr. Phys. **48**, 823 (2000).

[88] A. Sondberg Sørensen and K. Mølmer, Phys. Rev. A **66**, 022314 (2002).

[89] D. F. James and J. Jerke, Can. J. Phys. **85**, 625 (2007).

[90] O. Gamel and D. F. V. James, Phys. Rev. A **82**, 052106 (2010).

[91] C. E. Theodosiou, Phys. Rev. A **30**, 2881 (1984).

[92] I. I. Beterov, I. I. Ryabtsev, D. B. Tretyakov, and V. M. Entin, Phys. Rev. A **79**, 052504 (2009).

[93] C. S. E. van Ditzhuijzen, A. F. Koenderink, J. V. Hernández, F. Robicheaux, L. D. Noordam, and H. B. van Linden van den Heuvell, Phys. Rev. Lett. **100**, 243201 (2008).

[94] A. Paris-Mandoki, H. Gorniaczyk, C. Tresp, I. Mirgorodskiy, and S. Hofferberth, J. Phys. B: At., Mol. Opt. Phys. **49**, 164001 (2016).

[95] T. G. Walker and M. Saffman, Phys. Rev. A **77**, 032723 (2008).

[96] F. M. Gambetta, W. Li, F. Schmidt-Kaler, and I. Lesanovsky, Phys. Rev. Lett. **124**, 043402 (2020).

[97] C. Zhang, F. Pokorny, W. Li, G. Higgins, A. Pöschl, I. Lesanovsky, and M. Hennrich, Nature (London) **580**, 345 (2020).

[98] J. Qian, Y. Qian, M. Ke, X.-L. Feng, C. H. Oh, and Y. Wang, Phys. Rev. A **80**, 053413 (2009); X.-F. Shi, Phys. Rev. Appl. **11**, 044035 (2019).

[99] E. Sjöqvist, D. M. Tong, L. M. Andersson, B. Hessmo, M. Johansson, and K. Singh, New J. Phys. **14**, 103035 (2012).

[100] G. F. Xu, J. Zhang, D. M. Tong, E. Sjöqvist, and L. C. Kwek, Phys. Rev. Lett. **109**, 170501 (2012).

[101] Z.-Y. Xue, J. Zhou, Y.-M. Chu, and Y. Hu, Phys. Rev. A **94**, 022331 (2016).

[102] P. Z. Zhao, X.-D. Cui, G. F. Xu, E. Sjöqvist, and D. M. Tong, Phys. Rev. A **96**, 052316 (2017).

[103] B.-J. Liu, X.-K. Song, Z.-Y. Xue, X. Wang, and M.-H. Yung, Phys. Rev. Lett. **123**, 100501 (2019).

[104] Y. Aharonov and J. Anandan, Phys. Rev. Lett. **58**, 1593 (1987).

[105] D. D. B. Rao and K. Mølmer, Phys. Rev. Lett. **111**, 033606 (2013).

[106] S. de Léséleuc, D. Barredo, V. Lienhard, A. Browaeys, and T. Lahaye, Phys. Rev. Lett. **119**, 053202 (2017).

[107] K. Afrousheh, P. Bohlouli-Zanjani, D. Vagale, A. Mugford, M. Fedorov, and J. D. D. Martin, Phys. Rev. Lett. **93**, 233001 (2004).

[108] S. Sevinçli and T. Pohl, New J. Phys. **16**, 123036 (2014).

[109] M. Marcuzzi, E. Levi, W. Li, J. P. Garrahan, B. Olmos, and I. Lesanovsky, New J. Phys. **17**, 072003 (2015).

[110] T. G. Walker and M. Saffman, J. Phys. B: At., Mol. Opt. Phys. **38**, S309 (2005).

[111] T. Vogt, M. Viteau, A. Chotia, J. Zhao, D. Comparat, and P. Pillet, Phys. Rev. Lett. **99**, 073002 (2007).

[112] I. I. Ryabtsev, D. B. Tretyakov, I. I. Beterov, and V. M. Entin, Phys. Rev. Lett. **104**, 073003 (2010).